Available online at www.sciencedirect.com
SCIENCE DIRECT®
International Journal of Heat and Mass Transfer 49 (2006) 3034–3044
International Journal of HEAT and MASS TRANSFER
www.elsevier.com/locate/ijhmt

Investigation of natural-convection heat transfer coefficient on a vertical square fin of finned-tube heat exchangers

Han-Taw Chen *, Jui-Che Chou

Department of Mechanical Engineering, National Cheng Kung University, Tainan 701, Taiwan, ROC

Received 26 August 2005; received in revised form 3 February 2006
Available online 19 April 2006

Abstract

The finite difference method in conjunction with the least-squares scheme and the experimental temperature data is proposed to predict the average natural-convection heat transfer coefficient and the fin efficiency on a vertical square fin of one-circular tube plate finned-tube heat exchangers. In the present study, the radiation and convection heat transfer coefficients are simultaneously taken into consideration. The heat transfer coefficient on this square fin is very non-uniform. Thus the whole plate fin is divided into several sub-fin regions in order to predict the average heat transfer coefficient $\bar{h}$ and the fin efficiency on the fin from the knowledge of the fin temperature recordings at several selected measurement locations. The results show that the heat transfer coefficient on the bottom fin region of the tube can be markedly higher than that on the top fin region of the tube. The $\bar{h}$ value increases with the fin spacing S and approaches an asymptotical value obtained from a single square fin as $S \to \infty$. The fin temperature distributions depart from the ideal isothermal situation and the fin temperature decreases more rapidly away from the circular center with increasing the fin spacing. In order to show the accuracy of the present inverse scheme, a comparison of the average heat transfer coefficient on the fin between the present predicated results and those obtained from the correlation recommended by current textbooks is made.

1. Introduction

The fins in heat exchangers are always applied to increase the heat flow per unit of basic surface. The analysis of a continuous plate fin pierced by a regularly spaced array of circular tubes in staggered and in-line arrays has many engineering applications [1]. In order to simplify the problem considered, the calculation of the standard fin efficiency usually assumes that the heat transfer coefficient is constant over the plate fin. However, it is well known that there exists a very complex flow pattern within a plate finned-tube heat exchanger due to a plume of the heated air rising above the horizontal circular tube in natural convection. The boundary layer over a horizontal hot tube starts to develop at the bottom of the tube and increases in thickness along the circumference. The flow forms a low-velocity region above the tube. Thus the heat transfer coefficient is highest on the bottom region of the tube and is lowest on the top region of the tube. This causes local variations of the heat transfer coefficient on the fin. On the other hand, the heat transfer coefficient on the fin is very non-uniform. This implies that the actual steady-state heat transfer coefficient on the fin inside a plate finned-tube heat exchanger should be the function of position. As shown in Ref. [2], the measurements of the local heat transfer coefficient on plain fins under steady-state heat transfer conditions are very difficult to perform, since the local fin temperature and local heat flux are required. Thus the estimation of a more accurate heat transfer coefficient on the fin is an important task for the device of the high-performance heat exchangers.

Quantitative studies of the heat transfer processes occurring in the industrial applications require accurate knowledge of the surface conditions and the thermal physical quantities of the material. It is well known that these

* Corresponding author. Fax: +886 6 235 2973.
E-mail address: htchen@mail.ncku.edu.tw (H.-T. Chen).

0017-9310/$ - see front matter © 2006 Elsevier Ltd. All rights reserved.
doi:10.1016/j.ijheatmasstransfer.2006.02.009

Nomenclature

A_f	area of the whole plate fin, m^2
A_j	area of the jth sub-fin region, m^2
$[A]$	global conduction matrix
d_o	outer diameter of a tube, m
$[F]$	force matrix
h	local heat transfer coefficient, W/m^2 K
$\bar{h}$	unknown average heat transfer coefficient on the whole plate fin, W/m^2 K
$\bar{h}_j$	unknown average heat transfer coefficient on the jth sub-fin region, W/m^2 K
k	thermal conductivity of the fin, W/m K
k_{air}	thermal conductivity of the air, W/m K
L	side length of a square fin, m
ℓ	distance between two neighboring nodes in the x- and y-directions
m	dimensionless parameter defined in Eq. (5)
$\bar{m}_j$	unknown dimensionless parameter on the jth sub-fin region defined in Eq. (10)
N	number of sub-fin regions
Nu_s	Nusselt number defined in Eq. (37)
N_x	number of nodes in the x-direction
N_y	number of nodes in the y-direction
Q	total heat rate dissipated from the whole plate fin, W
q_j	heat rate dissipated from the jth sub-fin region, W
Ra_s	Rayleigh number defined in Eq. (36)
r_o	outer radius of the circular tube, m
S	fin spacing, m
S_1	outer boundary surface of the circular tube
T	fin temperature, K
T_j	temperature measurement on the jth sub-fin region, K
T_o	outer surface temperature of the circular tube, K
T_∞	ambient temperature, K
X, Y	spatial coordinates, m
x, y	dimensionless spatial coordinates

Greek symbols

α	thermal diffusivity of the air, m^2/s
β	volumetric thermal expansion coefficient, 1/K
δ	fin thickness, m
η_f	fin efficiency
ν	kinematic viscosity of the air, m^2/s
θ	temperature difference, $T - T_\infty$
$[\theta]$	global temperature matrix

Superscripts

cal	calculated value
mea	measured data

physical quantities and the surface conditions can be predicted using the temperature measurements inside the material. Such problems are called the inverse heat conduction problems and have become an interesting subject recently. To date, various inverse methods in conjunction with the measured temperatures inside the test material have been developed for the analysis of the inverse heat conduction problems [3,4]. However, to the authors' knowledge, a few investigators performed the prediction of the local heat transfer coefficients on a fin inside the plate finned-tube heat exchangers.

Lin et al. [5] used the finite difference method in conjunction with the linear least-squares scheme to estimate the space-variable heat transfer coefficient on a heated cylinder normal to the laminar and turbulent air streams. Owing to the requirement of the local fin temperature measurements, the estimations of the local heat transfer coefficients on the plate fin under steady-state heat transfer conditions are generally more difficult than those on the boundary surface of a physical geometry, as shown in Ref. [5]. Thus a few researchers predicted the distribution of the local heat transfer coefficients on a plate fin [6–11]. Jones and Russell [6] applied the transient technique to determine the local heat transfer coefficients on the rectangular fin pierced by an elliptical steel tube and then the finite element method was used to calculate its fin efficiency. Saboya and Sparrow [7] and Rosman et al. [8] cast solid naphthalene plates in the form of a plate-fin-and-tube flow passage and used mass transfer techniques to infer the local heat transfer coefficients from the heat-mass transfer analogy. The local mass transfer coefficients were defined by measuring the thickness of naphthalene lost by sublimation during a timed test run. Recently, Ay et al. [9] performed an experimental study with the infrared thermovision to monitor the temperature distribution on a plate-fin surface inside the plate finned-tube heat exchangers, and then the local heat transfer coefficients on the test fin can be determined using the obtained experimental temperature measurements. Huang et al. [10] applied the steepest descent method and a general purpose commercial code CFX4.4 to estimate the local heat transfer coefficients for the plate finned-tube heat exchangers based on the simulated measured temperature distribution on the fin surface by infrared thermography. However, the difference of the local heat transfer coefficients in the wake and frontal regions of the tube and the fin efficiency on the fin inside the plate finned-tube heat exchangers are not shown in the works of Ay et al. [9] and Huang et al. [10]. Sometimes, it is may be difficult to measure the temperature distributions on the fin of plate finned-tube heat exchangers using the infrared thermography and the thermocouples for some practical heat transfer problems. Recently, Chen et al. [11] applied

the finite difference method in conjunction with the least-squares scheme and the experimental temperature data to predict the fin efficiency and the average heat transfer coefficient on the fin inside one-tube plate finned-tube heat exchangers for various air speeds. The present study will apply the similar method proposed by Chen et al. [11] to estimate the fin efficiency and the average heat transfer coefficient on the fin inside one-tube plate finned-tube heat exchangers in natural convection. The present estimated results of the average natural-convection heat transfer coefficient on the fin will compare with those obtained from the correlation recommended by current textbooks.

The inverse analysis of the present study is that the whole fin area is divided into several analysis sub-fin regions and then the fin temperatures at these selected measurement locations are measured using T-type thermocouples. Afterwards, the finite difference method in conjunction with these temperature measurements and the least-squares method is applied to predict the average heat transfer coefficients on these sub-fin regions. Furthermore, the average heat transfer coefficient on the whole plate fin $\bar{h}$ and the fin efficiency can be obtained for various values of the fin spacing under the given conditions of the ambient temperature and the tube temperature.

The advantage of the present study is that the governing differential equations for the airflow do not need to be solved. In this study, the effect of the fin spacing on the estimation of the $\bar{h}$ value will be investigated. The computational procedure for the estimates of the heat transfer coefficients on each sub-fin region is performed repeatedly until the sum of the squares of the deviations between the calculated and measured temperatures becomes minimum.

2. Mathematical formulation

The experimental apparatus configuration of the present study is shown in Fig. 1. The schematic diagram of one-tube plate fin heat exchanger in natural convection is shown in Fig. 2. Fig. 3 shows the physical model of the two-dimensional thin plate fin inside one-tube plate fin heat exchanger, where r_o, L and δ denote the outer radius of the circular tube, the side length of the square plate fin and the fin thickness, respectively. The circular center is located at

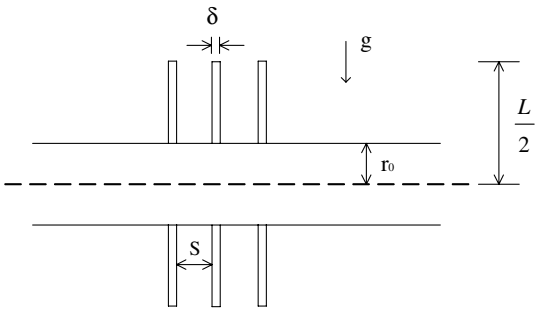

Fig. 2. Schematic diagram of one-tube plate fin heat exchangers with the fin spacing.

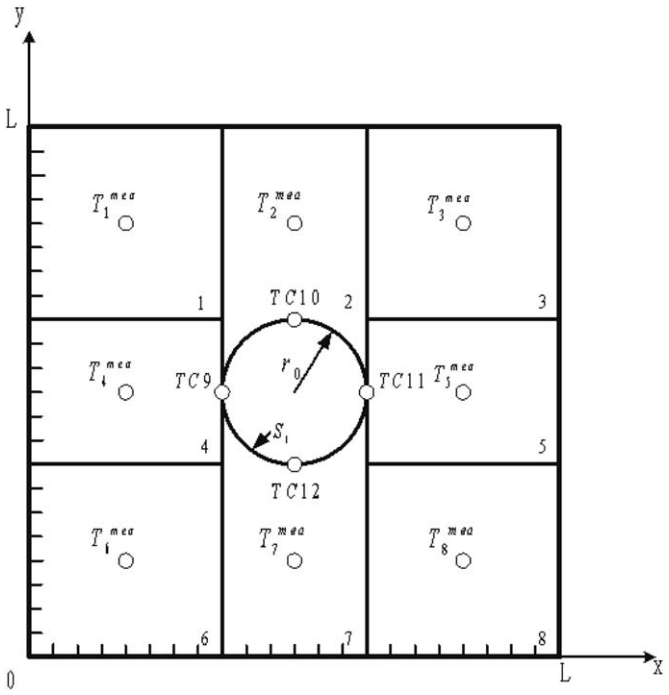

Fig. 3. Physical geometry of two-dimensional plate fin with a circular tube.

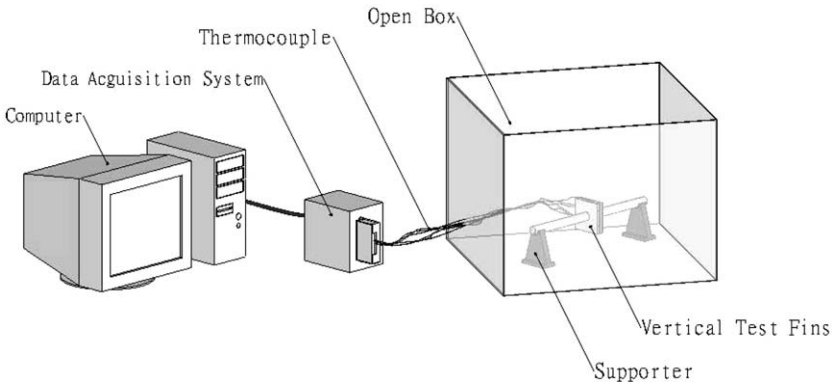

Fig. 1. Experimental apparatus for the temperature measurements of a vertical fin of finned-tube heat exchangers.

$(L/2, L/2)$. T_o and T_∞ respectively denote the outer surface temperature of the circular tube and the ambient temperature. Owing to the thin fin behavior, the temperature gradient in the z-direction (the fin thickness) is small and the fin temperature varies only in the X- and Y-directions. The "insulated tip" assumption can be an adequate approximation provided that the actual heat flux dissipated through the tip is much smaller than the total heat flux drawn from the base wall [12]. The heat transfer coefficient $h(X, Y)$ in the present study is assumed to be non-uniform. This heat transfer coefficient on the fin inside a plate finned-tube heat exchanger can be estimated provided that the fin temperatures at various measurement locations can be measured. Under the assumptions of the steady-state heat transfer conditions and constant thermal properties, the two-dimensional heat conduction equation for the continuous thin fin inside one-tube plate finned-tube heat exchanger can be expressed as

$$\frac{\partial^2 T}{\partial X^2}+\frac{\partial^2 T}{\partial Y^2}=\frac{2h(X,Y)}{k\delta}(T-T_\infty) \tag{1}$$

Its corresponding boundary conditions are

$$\frac{\partial T}{\partial X}=0 \quad \text{at } X=0 \text{ and } X=L \tag{2}$$

$$\frac{\partial T}{\partial Y}=0 \quad \text{at } Y=0 \text{ and } Y=L \tag{3}$$

$$T=T_o \quad (X,Y) \text{ on } S_1 \tag{4}$$

where T is the fin temperature. X and Y are Cartesian coordinates. S_1 denotes the boundary of the circular tube with radius $r_o \cdot k$ is the thermal conductivity of the fin.

For convenience of the inverse analysis, the following dimensionless parameters are introduced as

$$x=X/L, \quad y=Y/L \quad \text{and} \quad m(x,y)=\frac{2L^2h(x,y)}{k\delta} \tag{5}$$

Substitution of Eq. (5) into Eqs. (1)–(4) gives the following equations.

$$\frac{\partial^2\theta}{\partial x^2}+\frac{\partial^2\theta}{\partial y^2}=m(x,y)\theta \tag{6}$$

$$\frac{\partial\theta}{\partial x}=0 \quad \text{at } x=0 \text{ and } x=1 \tag{7}$$

$$\frac{\partial\theta}{\partial y}=0 \quad \text{at } y=0 \text{ and } y=1 \tag{8}$$

and

$$\theta=\theta_0 \quad (x,y) \text{ on } S_1 \tag{9}$$

where $\theta=T-T_\infty$.

3. Numerical analysis

In the present study, the whole plate fin is divided into N sub-fin regions. The heat transfer coefficient on each sub-fin region is assumed to be constant. Thus the application of the finite difference method to Eq. (6) can produce the following difference equation on the kth sub-fin region as

$$\frac{\theta_{i+1,j}-2\theta_{i,j}+\theta_{i-1,j}}{\ell^2}+\frac{\theta_{i,j+1}-2\theta_{i,j}+\theta_{i,j-1}}{\ell^2}=\bar{m}_k\theta_{i,j} \quad \text{for } k=1,2,\ldots,N \tag{10}$$

where ℓ is the distance between two neighboring nodes in the x- and y-directions and is defined as $\ell=1/(N_x-1)=1/(N_y-1)$. N_x and N_y are the nodal numbers in x- and y-directions, respectively. $\bar{m}_k$ denotes the unknown dimensionless parameter on the kth sub-fin region and is defined as $\bar{m}_k=2L^2\bar{h}_k/(k\delta)$. $\bar{h}_k$ denotes the average heat transfer coefficient on the kth sub-fin region.

The application of the central difference approximation to the boundary conditions (7) and (8) can yield their approximate forms as

$$\theta_{2,j}=\theta_{0,j} \quad \text{and} \quad \theta_{N_x-1,j}=\theta_{N_x+1,j} \quad \text{for } j=1,2,\ldots,N_y \tag{11}$$

$$\theta_{i,2}=\theta_{i,0} \quad \text{and} \quad \theta_{i,N_y-1}=\theta_{i,N_y+1} \quad \text{for } i=1,2,\ldots,N_x \tag{12}$$

Substitution of Eqs. (11) and (12) into their corresponding difference equations can obtain the difference equations at the boundary surfaces as

$$\frac{2\theta_{2,j}-2\theta_{1,j}}{\ell^2}+\frac{\theta_{1,j+1}-2\theta_{1,j}+\theta_{1,j-1}}{\ell^2}=\bar{m}_k\theta_{1,j} \quad \text{for } k=1,4,6 \tag{13}$$

$$\frac{-2\theta_{N_x,j}+2\theta_{N_x-1,j}}{\ell^2}+\frac{\theta_{N_x,j+1}-2\theta_{N_x,j}+\theta_{N_x,j-1}}{\ell^2}=\bar{m}_k\theta_{N_x,j} \quad \text{for } k=3,5,8 \tag{14}$$

$$\frac{\theta_{i+1,1}-2\theta_{i,1}+\theta_{i-1,1}}{\ell^2}+\frac{2\theta_{i,2}-2\theta_{i,1}}{\ell^2}=\bar{m}_k\theta_{i,1} \quad \text{for } k=6,7,8 \tag{15}$$

and

$$\frac{\theta_{i+1,N_y}-2\theta_{i,N_y}+\theta_{i-1,N_y}}{\ell^2}+\frac{-2\theta_{i,N_y}+2\theta_{i,N_y-1}}{\ell^2}=\bar{m}_k\theta_{i,N_y} \quad \text{for } k=1,2,3 \tag{16}$$

It can be found from Refs. [13,14] that the boundary of the circular tube may be approximated by an octagon in terms of a Cartesian coordinate system. Thus a more accurate modified difference equation based on this technique will be constructed in the present study.

The difference equations for the nodes at the interface of two neighboring sub-fin regions, as shown in Fig. 4, can be expressed as

$$\frac{\theta_{i+1,j}-2\theta_{i,j}+\theta_{i-1,j}}{\ell^2}+\frac{\theta_{i,j+1}-2\theta_{i,j}+\theta_{i,j-1}}{\ell^2}=\frac{\bar{m}_k+\bar{m}_{k^*}}{2}\theta_{i,j} \tag{17}$$

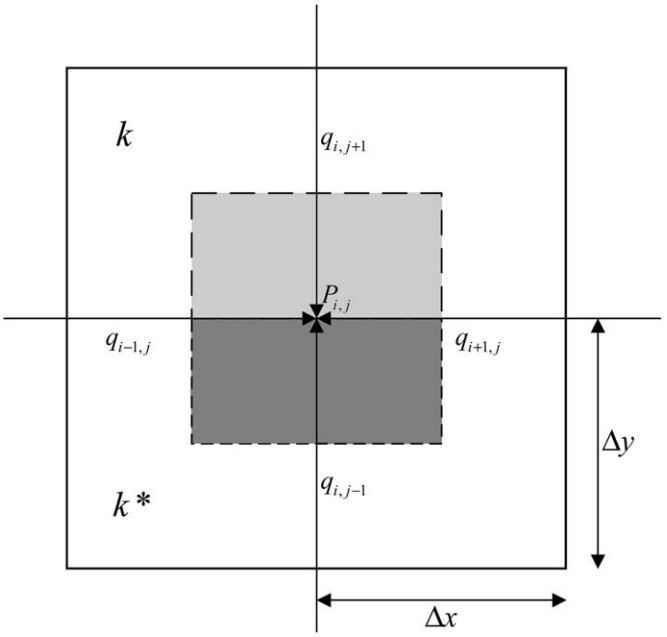

Fig. 4. Nodes for the interface of two-neighboring sub-fin areas.

Rearrangement of Eq. (10) and Eqs. (13)–(17) in conjunction with the difference equations in the neighboring of the circular tube can yield the following matrix equation.

$$[A][\theta] = [F] \tag{18}$$

where $[A]$ is a global conduction matrix. $[\theta]$ is a matrix representing the nodal temperatures. $[F]$ is a force matrix. The nodal temperatures can be obtained from Eq. (18) by using the Gauss elimination method.

However, it is may be difficult to measure the temperature distribution on the whole plate fin using the infrared thermography and the thermocouples for some practical heat transfer problems. Relatively, the unknown heat transfer coefficient $h(x,y)$ on a fin is not easy to be obtained. Under this circumstance, the whole plate fin considered can be divided into several sub-fin regions in the present inverse scheme and then the unknown heat transfer coefficient on each sub-fin region can be approximated by a constant value. Under this assumption, the heat rate dissipated from this sub-fin region q_j is

$$q_j = 2\bar{h}_j \int_{A_j} (T - T_\infty)\,\mathrm{d}A \quad \text{for } j = 1,2,\ldots,N \tag{19}$$

The average heat transfer coefficient on the whole plate fin $\bar{h}$ can be expressed as

$$\bar{h} = \sum_{j=1}^{N} \bar{h}_j A_j / A_\mathrm{f} \tag{20}$$

where N is the total number of the sub-fin regions. A_f is the area of the whole plate fin.

The efficiency of the continuous plate fin η_f is defined as the ratio of the actual heat transfer from the continuous plate fin to the dissipated heat from the fin maintained at the tube temperature T_o. Thus the fin efficiency η_f can be expressed as

$$\eta_\mathrm{f} = \frac{\sum_{j=1}^{N} q_j}{2A_\mathrm{f}(T_\mathrm{o} - T_\infty)\bar{h}} \tag{21}$$

The total heat rate dissipated from the whole plate fin to the ambient Q can be written as

$$Q = \sum_{j=1}^{N} q_j \tag{22}$$

In order to estimate the unknown heat transfer coefficient on the jth sub-fin region $\bar{h}_j$, the additional information of the steady-state temperature measurements at N interior measurement locations is required. The more a number of the sub-fin regions are, the more accurate the estimation of the unknown average heat transfer coefficient on the whole plate fin is. Relatively, a more computational time can be required. In the present study, T-type thermocouples are used to record the temperature information at selected measurement locations. The temperature measurement taken from the jth thermocouple is denoted by T_j^{mea} $(j = 1,\ldots,N)$, as shown in Table 1.

The least-squares minimization technique is applied to minimize the sum of the squares of the deviations between the calculated temperatures and the temperature measurements at selected measurement locations. The error in the estimates $E(\bar{m}_1,\bar{m}_2,\ldots,\bar{m}_N)$ will be minimized. $E(\bar{m}_1, \bar{m}_2,\ldots,\bar{m}_N)$ is defined as

$$E(\bar{m}_1,\bar{m}_2,\ldots,\bar{m}_N) = \sum_{j=1}^{N} [\theta_j^{\mathrm{cal}} - \theta_j^{\mathrm{mea}}]^2 \tag{23}$$

where the unknown average heat transfer coefficient on each sub-fin region h_i, $i = 1,2,\ldots,N$, can be obtained from the definition of $\bar{m}_i$. The calculated temperature taken from the jth thermocouple location, θ_j^{cal}, is taken from Eq. (18). The temperature θ_j^{mea} is defined as $\theta_j^{\mathrm{mea}} = T_j^{\mathrm{mea}} - T_\infty$.

The estimated values of $\bar{m}_i, i = 1,2,\ldots,N$, are determined until the value of $E(\bar{m}_1,\bar{m}_2,\ldots,\bar{m}_N)$ is minimum. The computational procedures for estimating the $\bar{m}_i$ value, $i = 1,2,\ldots,N$, are described as follows.

First, the initial guesses of $\bar{m}_i$, $i = 1,2,\ldots,N$, are arbitrarily chosen. Accordingly, the calculated temperature θ_j^{cal} can be determined. Deviation of θ_j^{mea} and θ_j^{cal}, e_j, is expressed as

$$e_j = \theta_j^{\mathrm{cal}} - \theta_j^{\mathrm{mea}} \quad \text{for } j = 1,2,\ldots,N \tag{24}$$

The new calculated temperature $\theta_j^{\mathrm{cal},n}$ can be expanded in a first-order Taylor series as

$$\theta_j^{\mathrm{cal},n} = \theta_j^{\mathrm{cal}} + \sum_{i=1}^{N} \frac{\partial \theta_j^{\mathrm{cal}}}{\partial \bar{m}_i} d\bar{m}_i \quad \text{for } j = 1,2,\ldots,N \tag{25}$$

In order to obtain the $\frac{\partial \theta_j^{\mathrm{cal}}}{\partial \bar{m}_i}$ value, the new estimated value $\bar{m}_i^*$ is introduced and is expressed as

$$\bar{m}_i^* = \bar{m}_i + d_i\delta_{ik} \quad \text{for } i,k = 1,2,\ldots,N \tag{26}$$

Table 1
Temperature measurements and the present estimates for various T_0, T_∞ and S values

	$S = 0.005$ m $T_0 = 343.029$ K, $T_\infty = 303$ K	$S = 0.01$ m $T_0 = 342.585$ K, $T_\infty = 301$ K	$S = 0.02$ m $T_0 = 340.692$ K, $T_\infty = 299$ K	$S \to \infty$ $T_0 = 345.49$ K, $T_\infty = 299$ K
T_j^{mea} (K)	$T_1^{mea} = 323.238$	$T_1^{mea} = 319.02$	$T_1^{mea} = 313.172$	$T_1^{mea} = 313.576$
	$T_2^{mea} = 330.78$	$T_2^{mea} = 327.546$	$T_2^{mea} = 321.234$	$T_2^{mea} = 323.424$
	$T_3^{mea} = 325.309$	$T_3^{mea} = 318.705$	$T_3^{mea} = 313.872$	$T_3^{mea} = 313.125$
	$T_4^{mea} = 321.401$	$T_4^{mea} = 317.608$	$T_4^{mea} = 312.941$	$T_4^{mea} = 314.055$
	$T_5^{mea} = 323.024$	$T_5^{mea} = 316.309$	$T_5^{mea} = 312.815$	$T_5^{mea} = 312.256$
	$T_6^{mea} = 315.276$	$T_6^{mea} = 311.04$	$T_6^{mea} = 307.083$	$T_6^{mea} = 308.817$
	$T_7^{mea} = 317.771$	$T_7^{mea} = 314.549$	$T_7^{mea} = 309.255$	$T_7^{mea} = 311.032$
	$T_8^{mea} = 314.194$	$T_8^{mea} = 309.95$	$T_8^{mea} = 305.979$	$T_8^{mea} = 306.703$
$\bar{h}_j$ (W/m^2 K)	$\bar{h}_1 = 3.341$	$\bar{h}_1 = 4.763$	$\bar{h}_1 = 6.500$	$\bar{h}_1 = 8.135$
	$\bar{h}_2 = 0.919$	$\bar{h}_2 = 0.252$	$\bar{h}_2 = 4.540$	$\bar{h}_2 = 2.940$
	$\bar{h}_3 = 2.242$	$\bar{h}_3 = 4.471$	$\bar{h}_3 = 5.379$	$\bar{h}_3 = 7.815$
	$\bar{h}_4 = 15.213$	$\bar{h}_4 = 19.154$	$\bar{h}_4 = 25.267$	$\bar{h}_4 = 27.149$
	$\bar{h}_5 = 11.094$	$\bar{h}_5 = 22.958$	$\bar{h}_5 = 25.306$	$\bar{h}_5 = 33.459$
	$\bar{h}_6 = 7.210$	$\bar{h}_6 = 10.492$	$\bar{h}_6 = 10.997$	$\bar{h}_6 = 8.808$
	$\bar{h}_7 = 20.915$	$\bar{h}_7 = 23.832$	$\bar{h}_7 = 39.110$	$\bar{h}_7 = 36.189$
	$\bar{h}_8 = 10.755$	$\bar{h}_8 = 12.546$	$\bar{h}_8 = 15.252$	$\bar{h}_8 = 13.958$
q_j (W)	$q_1 = 0.182$	$q_1 = 0.234$	$q_1 = 0.256$	$q_1 = 0.308$
	$q_2 = 0.054$	$q_2 = 0.014$	$q_2 = 0.216$	$q_2 = 0.224$
	$q_3 = 0.132$	$q_3 = 0.214$	$q_3 = 0.220$	$q_3 = 0.300$
	$q_4 = 0.618$	$q_4 = 0.726$	$q_4 = 0.842$	$q_4 = 1.014$
	$q_5 = 0.678$	$q_5 = 0.824$	$q_5 = 0.838$	$q_5 = 1.134$
	$q_6 = 0.248$	$q_6 = 0.304$	$q_6 = 0.260$	$q_6 = 0.248$
	$q_7 = 0.724$	$q_7 = 0.768$	$q_7 = 1.034$	$q_7 = 1.102$
	$q_8 = 0.346$	$q_8 = 0.330$	$q_8 = 0.322$	$q_8 = 0.322$
$\bar{h}$ (W/m^2 K)	8.562	11.708	15.648	16.273
Q (W)	2.782	3.416	3.988	4.586
η	0.440	0.380	0.331	0.328

where $d_i = \bar{m}_i^* - \bar{m}_i$ denotes the correction. The symbol δ_{jk} is Kronecker delta.

Accordingly, the new calculated temperature $\theta_j^{cal,n}$ with respect to $\bar{m}_i^*$ can be determined from Eq. (18). Deviation of $\theta_j^{cal,n}$ and θ_j^{mea}, e_j^n, can be defined as

$$e_j^n = \theta_j^{cal,n} - \theta_j^{mea} \quad \text{for } j = 1, 2, \ldots, N \tag{27}$$

The finite difference representation of the derivative $\frac{\partial \theta_j^{cal}}{\partial \bar{m}_i}$ can be expressed as

$$\omega_j^i = \frac{\partial \theta_j^{cal}}{\partial \bar{m}_i} = \frac{\theta_j^{cal,n} - \theta_j^{cal}}{\bar{m}_i^* - \bar{m}_i} \quad \text{for } j = 1, 2, \ldots, N \tag{28}$$

Substitution of Eqs. (24), (26) and (27) into Eq. (28) can yield

$$\omega_j^i = \frac{e_j^n - e_j}{d_i} \quad \text{for } j = 1, 2, \ldots, N \tag{29}$$

Substitution of Eq. (28) into Eq. (25) can obtain the new expression of $\theta_j^{cal,n}$ as

$$\theta_j^{cal,n} = \theta_j^{cal} + \sum_{i=1}^{N} \omega_j^i d_i^* \quad \text{for } j = 1, 2, \ldots, N \tag{30}$$

where $d_i^* = d\bar{m}_i$ denotes the new correction for the values of $\bar{m}_i$.

Substituting Eqs. (24) and (27) into Eq. (30) gives

$$e_j^n = e_j + \sum_{i=1}^{N} \omega_j^i d_i^* \quad \text{for } j = 1, 2, \ldots, N \tag{31}$$

As shown in Eq. (23), the error in the estimates $E(\bar{m}_1 + \Delta\bar{m}_1, \bar{m}_2 + \Delta\bar{m}_2, \ldots, \bar{m}_N + \Delta\bar{m}_N)$ can be expressed as

$$\mathbf{E} = \sum_{j=1}^{N} (e_j^n)^2 \tag{32}$$

In order to yield the minimum value of $\mathbf{E}$ with respect to the $\bar{m}_i$ values, differentiating $\mathbf{E}$ with respect to the new correction d_i^* will be performed. Thus the correction equations for the $\bar{m}_i$ values can be expressed as

$$\sum_{j=1}^{N} \sum_{k=1}^{N} \omega_k^i \omega_k^j d_j^* = -\sum_{j=1}^{N} \omega_j^i e_j \quad i = 1, 2, \ldots, N \tag{33}$$

Eq. (33) is a set of N algebraic equations for the new corrections. The new correction d_i^* can be obtained by solving Eq. (33). Furthermore, the new estimated heat transfer coefficients can also be determined. The above procedures are repeated until the values of $\left|\frac{\theta_j^{mea} - \theta_j^{cal}}{\theta_j^{mea}}\right|$, $j = 1, 2, \ldots, N$, are all less than 10^{-4}.

4. Experimental apparatus

The schematic diagram of the experimental apparatus used in the present study for the estimation of the natural-convection heat transfer coefficient on a square plate fin inside one-tube plate finned-tube heat exchangers is shown in Fig. 1. This experiment is conducted in an open

box, as shown in Fig. 1. This box with 550 mm in length, 450 mm in width and 300 mm in height is made of acrylic–plastic sheets. The horizontal circular tube with an outer diameter of 27.3 mm and 2 mm in thickness and the test square fin with 100 mm in length, 100 mm in width and 1 mm in thickness are made of AISI 304 stainless material. It can be found from Ref. [15] that the thermal conductivity of AISI 304 stainless material is 14.9 W/m K. The horizontal circular tube is placed on two wood supporters, which is 98 mm above an experimental table to prevent ground effects. The test fins are vertically mounted on this circular tube, as shown in Figs. 1 and 2. The ambient temperature and the test fin temperature are measured by using T-type thermocouples. A cylindrical rod with an outer diameter of 20 mm and 100 mm in length bound by a single thermofoil heater with an outer diameter of 1.5 mm is inserted in the circular tube and then the tube will be heated. Thus the radial gap between the surrounding circular tube and the whole electrical heating rod is small. On the other hand, the whole electrical heating rod is nearly fitted to the surrounding circular tube. Two hundred watts power input was supplied the heater. The electrical heating rod was heated about 2 h. However, the steady-state condition has reached about 2000 s. The readings of all the thermocouples used to measure the ambient air and the fin are recorded from $t = 0$ until the steady-state condition has reached. All the data signals were collected and converted by a data acquisition system (National Instruments NI SCXI-1000, 1102, 1300). The data acquisition system then transmitted the converted signals through a GPIB interface to a personal computer in conjunction with a Labview software for further operation. The accuracy of the thermocouple is ±0.4%. The histories of the temperature measurements for all the thermocouples are obtained by a curve-fitted scheme. The experiment will be repeatedly made provided that one of the temperature measurements for all the thermocouples is not very accurate. In order to check the accuracy of the temperature measurements, the experiments are at least repeated two times. In order to minimize the effect of the thermal contact resistance between the fin and the circular tube on the estimates, the gap between the fin and the circular tube is filled with a satlon cyanoacrylate adhesive. In addition, four thermocouples placed in the interface between the fin and the circular tube are fixed at four different positions of the fin base, TC9, TC10, TC11 and TC12 shown in Fig. 3, by using a satlon cyanoacrylate adhesive. The fin base temperatures are measured from these four thermocouples. There exists a plume of the heated air rising above the horizontal circular tube in the present problem. The boundary layer over a horizontal heated tube starts to develop at the bottom of the tube and increases in thickness along its circumference. Thus the flow forms a low-velocity region above the tube. This implies that the fin base temperatures at the positions of TC10 and T12, respectively are the highest temperature and the lowest temperature for these four temperature measurements. These four temperature measurements do not deviate much from each other. Thus the average of these four temperature measurements is taken as the fin base temperature and is also assumed to be the outer surface temperature of the circular tube T_0 in the present study. It can be observed from Table 1 that the fin temperatures on the top fin region of the tube are also markedly greater than those on the bottom fin region of the tube for various T_0, T_∞ and S values. The ambient temperature T_∞ is installed at 100 mm away from the test specimen. For the present problem, the flow and thermal fields in the previous works were often assumed to be symmetric. In order to investigate the reliability of the above assumption, the regular arrangements of the thermocouples welded on the fin are chosen. Thus the whole plate fin is divided into eight regions, i.e., $N = 8$. Regions 1–3 are the top area of the tube. Regions 6–8 are the bottom area of the tube. In order to estimate the average heat transfer coefficient on each sub-fin region, eight T-type thermocouples are welded at the suitable positions of the sub-fin region, as shown in Fig. 3. Eight T-type thermocouples for the measurements of the fin temperature are respectively welded at (2/11, 9/11), (1/2, 9/11), (9/11, 9/11), (2/11, 1/2), (9/11, 1/2), (2/11, 2/11), (1/2, 2/11) and (9/11, 2/11). It can be observed that the first, third, fourth, fifth, sixth and eighth thermocouples are symmetric with respect to $y = 1/2$. The diameter of the spot sizes of eight thermocouples is about 0.13 mm.

5. Results and discussion

It can be observed from Ref. [12] that the "insulated tip" assumption is a good approximation when the actual heat flux passed through the tip is negligible relative to the total heat flux drawn from the base wall. For simplicity, the average heat transfer coefficient on the tip surface can be assumed to be the same as that on the lateral surfaces of the fin. On the other hand, the "insulated tip" assumption will be reasonable provided that the surface area of the fin tip is very smaller than the total fin surface area. Their ratio for the present study can be written as $\frac{4\delta L}{(L^2-\pi r_0^2)+4\delta L}$. Based on the experiment data given in the present study, the surface area of the fin tip is only 4.07% of the total fin surface area. This implies that the heat flux passed through the fin tip can be neglected in the present study. Thus Eqs. (2) and (3) in the present study should be the reasonable assumptions. The values of $T_1^{\mathrm{mea}}(2/11, 9/11)$, $T_2^{\mathrm{mea}}(1/2, 9/11)$, $T_3^{\mathrm{mea}}(9/11, 9/11)$, $T_4^{\mathrm{mea}}(2/11, 1/2)$, $T_5^{\mathrm{mea}}(9/11, 1/2)$, $T_6^{\mathrm{mea}}(2/11, 2/11)$, $T_7^{\mathrm{mea}}(1/2, 2/11)$ and $T_8^{\mathrm{mea}}(9/11, 2/11)$, respectively denote T_1^{mea}, T_2^{mea}, T_3^{mea}, T_4^{mea}, T_5^{mea}, T_6^{mea}, T_7^{mea} and T_8^{mea}. It is obvious that eight thermocouples are installed at symmetric positions with respect to the center of the square plate fin. The temperature measurements T_1^{mea}, T_2^{mea}, T_3^{mea}, T_4^{mea}, T_5^{mea}, T_6^{mea}, T_7^{mea} and T_8^{mea} for various T_0, T_∞ and S values are shown in Table 1. Table 1 also shows the effect of the fin spacing S on the average heat transfer coefficient on the jth sub-fin region $\bar{h}_j$, heat rate on the jth sub-fin region q_j, total heat rate on the whole

plate fin Q, average heat transfer coefficient on the whole plate fin $\bar{h}$ and fin efficiency η_f. It is obvious that Table 1 shows $T_1^{mea} \neq T_3^{mea}$, $T_4^{mea} \neq T_5^{mea}$ and $T_6^{mea} \neq T_8^{mea}$. This phenomenon can result from the following reasons that the flow pattern of the present problem around the tube may become random in motion, and the test specimen cannot be horizontally positioned. Thus the symmetric assumptions of the flow and thermal fields cannot be very reasonable for the present real problem. Table 1 shows the heat transfer coefficient is highest on the bottom region of the tube and is lowest on the top region of the tube. It can be found from the textbook of Çengel [16] that the local Nusselt number is highest at the bottom of the tube and is lowest at the top of the tube. Obviously, the present estimates of $\bar{h}_j$ agree with this tendency. These results show that there exists a low-performance region on the top fin region of the tube, and the heat transfer coefficient on the fin is non-uniform. This also implies that the assumption of the constant heat transfer coefficient is not always reasonable for the present problem. The actual steady-state heat transfer coefficient on a fin inside a plate finned-tube heat exchanger should be the function of position. Therefore, in order to enhance the overall heat transfer, it is worth to find a way to increase heat transfer in the region 2. This may lead to design a heat exchanger with a high heat transfer performance. The ratio of the average heat transfer coefficient on the bottom fin region $\bar{h}_7$ to that on the top fin region $\bar{h}_2$ can be up to about 20 times for $S = 0.005$ m and is about 8.5 times for $S = 0.02$ m. This ratio can be decreased with increasing the fin spacing. The $\bar{h}$ value for $S = 0.02$ m is approximately 180% greater than that for $S = 0.005$ m. However, the Q value for $S = 0.02$ m is up to 43% greater than that for $S = 0.005$ m. Thus the effect of the fin spacing on $\bar{h}$ and Q is not negligent. It can be found from Table 1 that the heat rate on the top fin region of one-tube finned-tube heat exchanger in the range of $S \geqslant 0.005$ m is responsible for 2–5% of the total heat rate on the whole plate fin. The fin efficiency η_f in the range of $S \geqslant 0.005$ m decreases with increasing the S value. The η_f value decreases from 44% to 33%.

A resistance to the natural convective airflow in the fin arrays increases with decreasing the fin spacing for the present problem. This resistance can gradually decrease with increasing the fin spacing S and has a negligible effect on the average heat transfer coefficient for the fin spacing above a certain value. Thus the average heat transfer coefficient $\bar{h}$ increases with the fin spacing and approaches an asymptotical value obtained from a single square fin as $S \to \infty$. These results are shown in Fig. 5. The similar phenomenon can also be found from Ref. [17]. Figs. 6 and 7, respectively show the effect of the Rayleigh number Ra_s on the Nusselt number Nu_s and the fin efficiency η_f. The smoothing curves can be applied to match the data points of $Nu_s - Ra_s^{1/4}$ and $\eta_f - Ra_s^{1/4}$. The correlations of $Nu_s - Ra_s^{1/4}$ and $\eta_f - Ra_s^{1/4}$ can be obtained by using the least-square fitting method of experimental data and are expressed as

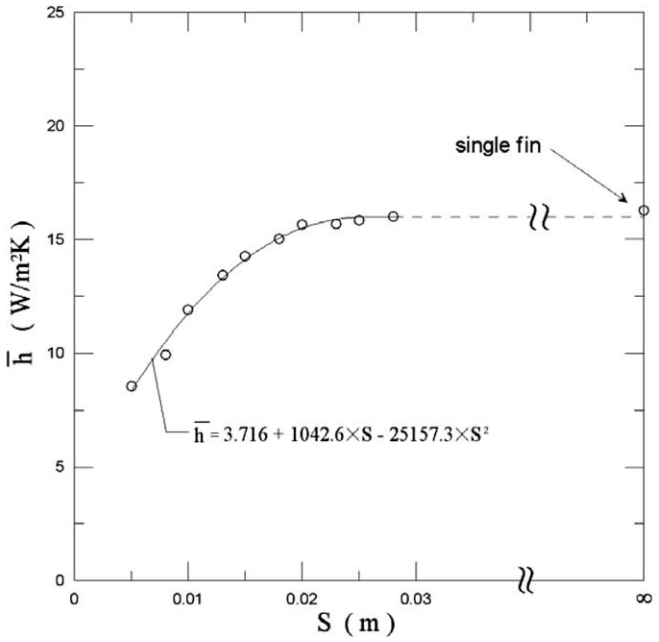

Fig. 5. Variation of $\bar{h}$ with S.

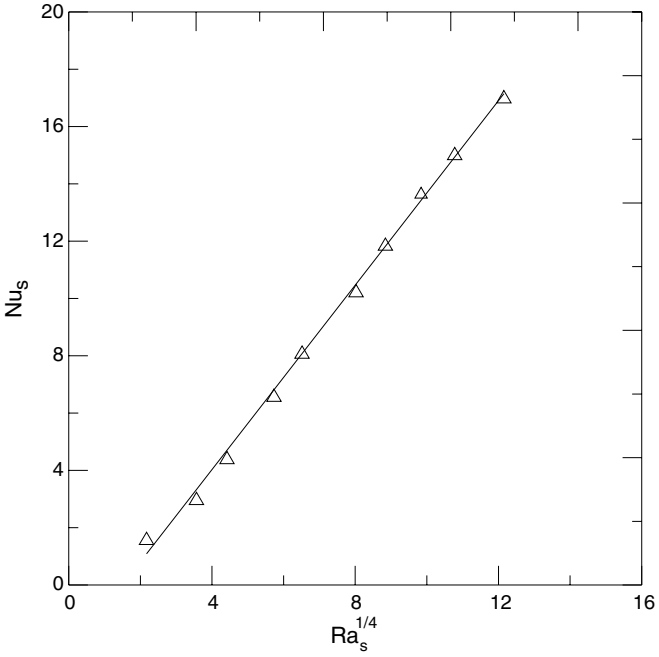

Fig. 6. Variation of Nu_s with $Ra_s^{1/4}$.

$$\eta_f = 0.546 - 0.057 \times (Ra_s^{1/4})^2 - 0.0001 \times (Ra_s^{1/4})^3 \quad (34)$$

and

$$Nu_s = 1.608 + 2.4 \times Ra_s^{1/4} \quad (35)$$

where the Raleigh number Ra_s and the Nusselt number Nu_s are defined as

$$Ra_s = \frac{g\beta(T_0 - T_\infty)S^3}{\nu\alpha}\left(\frac{S}{L}\right) \quad (36)$$

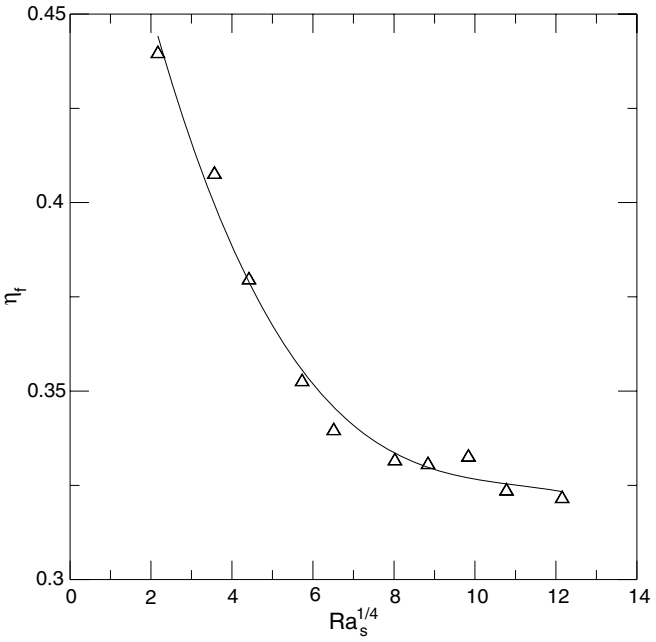

Fig. 7. Variation of η_f with $Ra_s^{1/4}$.

and

$$Nu_s = \frac{\bar{h}S}{k_{air}} \tag{37}$$

In Eqs. (36) and (37), k_{air} denotes the thermal conductivity of the air. The properties β, α and v, respectively denote the expansion coefficient, thermal diffusivity and kinematic viscosity of the air. Thus the Ra_s value ranges about from 22 to ∞ in this study.

It can be found from the textbook of Kreith and Bohn [15] and Raithby and Hollands [19] that the empirical relation of Nu_s and Ra_s in the range $0.2 < Ra_s < 4 \times 10^4$ for a square isothermal fin without the tube can be expressed as

$$\frac{\bar{h}S}{k_{air}} = \frac{QS}{2A_f(T_0 - T_\infty)k_{air}} = \left[\left(\frac{Ra_s^{0.89}}{18}\right)^{2.7} + (0.62Ra_s^{0.25})^{2.7}\right]^{1/2.7} \tag{38}$$

where properties are evaluated at the ambient temperature T_∞.

The empirical relation of Nu_s and Ra_s in the range $1.67 < \xi = D/d_0 < \infty$ for an annular circular isothermal fin can be expressed as [15,19]

$$Nu_s = \frac{Ra_{s,c}}{12\pi}[2 - \exp(-C^*) - \exp(-\beta^* C^*)] \tag{39}$$

where D is the outer diameter of the annular circular fin. All the properties are evaluated at the tube temperature T_0. C^*, β^* and $Ra_{s,c}$ are defined as

$$\beta^* = (0.17/\xi) + \exp(-4.8/\xi) \tag{40}$$

$$C^* = \frac{23.7 - 1.1[1 + (152/\xi^2)]^{1/2}}{1 + \beta^*} \frac{1}{Ra_{s,c}^{3/4}} \tag{41}$$

and

$$Ra_{s,c} = \frac{g\beta(T_0 - T_\infty)S^3}{v\alpha}\left(\frac{S}{D}\right) \tag{42}$$

It can also be found from the textbook of Kreith and Bohn [15] and Raithby and Hollands [19] that the Nusselt number relations from the lateral surfaces of the circular and square fins are equivalent if $D = 1.23L$.

It is known that heat is transferred to the surroundings by natural convection and radiation. On the other hand, the radiation heat transfer may be quite significant in natural convection [18]. However, the natural-convection heat loss can decrease more rapidly than the radiation heat loss with decreasing the fin spacing. It can be observed from Table 2 that the present estimates of $\bar{h}$ are higher than the empirical values obtained from Eq. (39) with $D = 1.23L$ for various S values. The above phenomena can result from the simultaneous consideration of the convection and radiation heat transfer coefficients and the non-isothermal situation of the fin temperature distribution in the present study. The results shown in Table 2 and Fig. 5 display that the asymptotical values of the $\bar{h}$ values obtained from the present inverse scheme and Eq. (39) with $D = 1.23L$ seem to approach those obtained from a single square fin as $S \to \infty$. This finding can lead to support the methodology of the present experiments and numerical analysis. However, the empirical values of $\bar{h}$ obtained from Eq. (38) are greater than the present estimates for

Table 2
Comparison of the heat transfer coefficient for various S and Ra_s values

S (m)	Ra_s	$\bar{h}$ (W/m^2 K)		
		Present estimates	Eq. (38)	Eq. (39) with $D = 1.23L$
0.005	22.169	8.562	7.892	3.212
0.008	161.589	9.939	17.398	5.033
0.01	381.38	11.708	29.156	5.391
0.013	1077.85	13.410	55.997	5.547
0.015	1799.8	14.253	76.399	5.591
0.018	4144.11	15.015	133.157	5.792
0.02	6110.96	15.648	169.787	5.817
0.025	18339.5	15.844	362.948	6.155

$S \geqslant 0.008$ m and are less than the present estimates for $S \leqslant 0.005$ m. In addition, the deviation of $\bar{h}$ between the present estimates and the empirical values obtained from Eq. (38) seems to increase with the fin spacing or the Ra_s value. This implies that Eq. (38) may be suitable for lower Ra_s values. Table 2 also shows that the $\bar{h}$ values obtained from the present inverse scheme and Eq. (39) with $D = 1.23L$ range from 8.562 $W/m^2 K$ to 15.844 $W/m^2 K$ and from 3.212 $W/m^2 K$ to 6.155 $W/m^2 K$ for $S \geqslant 0.005$ m, respectively. It can be found from the textbook of Kreith and Bohn [15] that the natural-convection heat transfer coefficient for the ambient air ranges from 6 $W/m^2 K$ to 30 $W/m^2 K$. It is obvious that the $\bar{h}$ values obtained from the present inverse scheme and Eq. (39) with $D = 1.23L$ lie in the range from 6 $W/m^2 K$ to 30 $W/m^2 K$. Thus the present estimated values of $\bar{h}$ are in good agreement with the limited comparable data in Refs. [15,19] and are obtained over a reasonably wide range of the fin spacing. This implies that the present estimates can extend the range of previously available data.

Once the average heat transfer coefficient on each sub-fin region can be obtained, the temperature distribution on the whole plate fin can also be determined from Eq. (18). The differences between the calculated temperatures and the measured temperatures are very small. Thus the calculated temperatures at various measurement locations are not shown in the revised manuscript. However, the calculated temperature distributions on the whole plate fin for various S values are shown in Figs. 8–10. It can be observed from Figs. 8–10 that there is a considerable temperature drop between the tube wall and the edge of the plate fin owing to the poor thermal conductivity of the steel fin. The fin temperature distributions obviously depart from the ideal isothermal situation, and the fin temperature decreases more rapidly away from the circular center for larger values of the fin spacing.

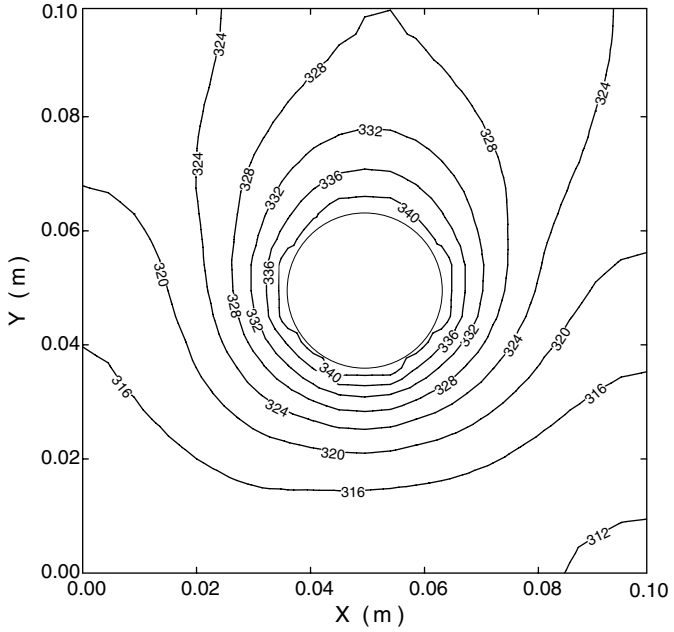

Fig. 8. Distribution of the calculated fin temperature for $S = 0.005$ m.

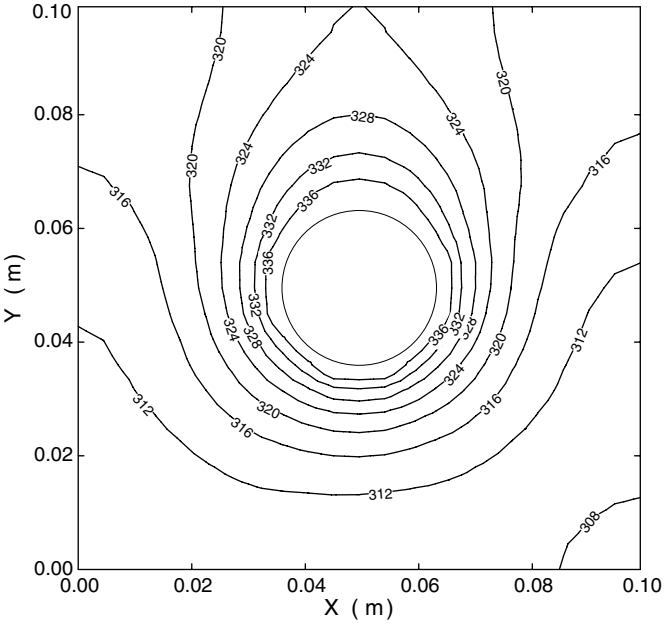

Fig. 9. Distribution of the calculated fin temperature for $S = 0.01$ m.

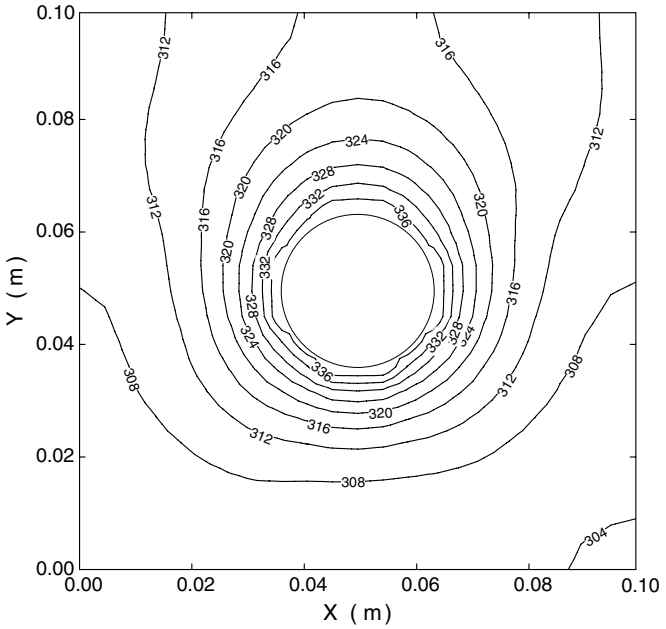

Fig. 10. Distribution of the calculated fin temperature for $S = 0.02$ m.

6. Conclusions

The present study proposes a numerical inverse scheme involving the finite-difference method in conjunction with the least-squares method and the experimental fin temperatures at eight measurement locations to estimate the unknown heat transfer coefficients on eight sub-fin regions,

the average heat transfer coefficient on the whole plate fin $\bar{h}$ and the fin efficiency η_f in natural convection for various T_0, T_∞ and S values. The estimated results show that the fin temperature distributions depart from the ideal isothermal situation. In addition, the fin temperature decreases more rapidly away from the circular center when the fin spacing increases. The average heat transfer coefficients are very low on the top fin region of the tube. The ratio of the average heat transfer coefficient on the bottom fin region to that on the top fin region can be up to about 20 times under the given conditions of T_o and T_∞. The $\bar{h}$ value increases with the fin spacing S and approaches an asymptotical value obtained from a single square fin as $S \to \infty$. The η_f value decreases with increasing the S value. The present estimated values of $\bar{h}$ can be obtained over a reasonably wide range of the fin spacing.

Acknowledgements

The authors gratefully acknowledge the financial support provided by the National Science Council of the Republic of China under Grant No. NSC 92-2622-E006-146.

References

[1] J.L. Lage, Tube-to-tube heat transfer degradation effect on finned-tube heat exchangers, Numer. Heat Transfer A 39 (2001) 321–337.
[2] R.L. Webb, Principles of Enhanced Heat Transfer, Wiley, New York, 1994, pp. 125–153.
[3] M.N. Özisik, Heat Conduction, second ed., Wiley, New York, 1993 (Chapter 14).
[4] K. Kurpisz, A.J. Nowak, Inverse Thermal Problems, Computational Mechanics Publications, Southampton, UK, 1995.
[5] J.H. Lin, C.K. Chen, Y.T. Yang, An inverse estimation of the thermal boundary behavior of a heated cylinder normal to a laminar air stream, Int. J. Heat Mass Transfer 43 (2000) 3991–4001.
[6] T.V. Jones, C.M.B. Russell, Efficiency of rectangular fins, in: ASME/AIChE National Heat Transfer Conference, Orlando, FL, 1980, pp. 27–30.
[7] F.E.M. Saboya, E.M. Sparrow, Local and average heat transfer coefficients for one-row plate fin and tube heat exchanger configurations, ASME J. Heat Transfer 96 (1974) 265–272.
[8] E.C. Rosman, P. Carajilescov, F.E.M. Saboya, Performance of one- and two-row tube and plate fin heat exchangers, ASME J. Heat Transfer 106 (1984) 627–632.
[9] H. Ay, J.Y. Jang, J.N. Yeh, Local heat transfer measurements of plate finned-tube heat exchangers by infrared thermography, Int. J. Heat Mass Transfer 45 (2002) 4069–4078.
[10] C.H. Huang, I.C. Yuan, H. Ay, A three-dimensional inverse problem in imaging the local heat transfer coefficients for plate finned-tube heat exchangers, Int. J. Heat Mass Transfer 46 (2003) 3629–3638.
[11] H.T. Chen, J.P. Song, Y.T. Wang, Prediction of heat transfer coefficient on the fin inside one-tube plate finned-tube heat exchangers, Int. J. Heat Mass Transfer 48 (2005) 2697–2707.
[12] A. Bejan, Heat Transfer, John Wiley & Sons, Inc., New York, 1993, pp. 53–62.
[13] H.T. Chen, J.T. Liou, Optimum dimensions of the continuous plate fin for various tube arrays, Numer. Heat Transfer A 34 (1998) 151–167.
[14] V.S. Arpaci, S.H. Kao, A. Selamet, Introduction to Heat Transfer, Prentice-Hall, NJ, 1999, pp. 202–205.
[15] F. Kreith, M.S. Bohn, Principles of Heat Transfer, fifth ed., West Publishing Co., New York, 1993.
[16] Y.A. Çengel, Heat Transfer—A Practical Approach, second ed., McGraw-Hill, New York, 2004.
[17] W. Elenbaas, Heat dissipation of parallel plates by free convection, Physica IX (1942) 1–28.
[18] C.D. Jones, L.F. Smith, Optimum arrangement of rectangular fins on horizontal surfaces for free convection heat transfer, ASME J. Heat Transfer 92 (1970) 6–10.
[19] G.D. Raithby, K.G.T. Hollands, Natural convection, in: W.M. Rohsenow, J.P. Hartnett, E.N. Ganic (Eds.), Handbook of Heat Transfer Fundamentals, second ed., McGraw-Hill, New York, 1985.